TEMPO-oxidized cellulose hydrogel for efficient adsorption of Cu 2+ and Pb 2+ modified by PEI

Xinyi Xing
Anhui Agricultural University
Wenqi Li
Anhui Agricultural University
Jie Zhang
Anhui Agricultural University
Han Wu
Anhui Agricultural University
Ying Guan
Anhui Agricultural University
Hui Gao (huigaozh@163.com)
Anhui Agricultural University

Research Article

Keywords: Poplar cellulose, Hydrogel, Heavy metal ions, Polyethylenimine modification

Posted Date: April 26th, 2021

DOI: https://doi.org/10.21203/rs.3.rs-383479/v1

Version of Record: A version of this preprint was published at Cellulose on July 7th, 2021. See the published version at https://doi.org/10.1007/s10570-021-04052-w.

Abstract

In this study, hydrogel were prepared by dissolving and regenerating *poplar*-cellulose in NaOH/urea/water system. The TEMPO-oxidized cellulose hydrogels (TCH) were prepared using microwave-assisted accelerated TEMPO-oxidation system. Polyethyleneimine (PEI) was grafted onto TCH with glutaraldehyde as a cross-linking agent and the products named as TCP. The hydrogels were characterized by SEM, FTIR, XPS and elemental analyzer. The maximum adsorption capacities of Cu^{2+} and Pb^{2+} by TCP were 109.89 mg/g and 279.32 mg/g, respectively. TCP was a single molecule adsorption process with better fitting of Langmuir model. Adsorption kinetics showed that the Pb^{2+} adsorption rate of TCP was higher than that for Cu^{2+}. The Cu^{2+} affinity of TCP was higher than the Pb^{2+}. The adsorption capacity of TCP for Cu^{2+} and Pb^{2+} was 58.26 mg/g and 91.96 mg/g, respectively, after five cycles. This study provided a promising option of preparing an efficient and recyclable adsorbent in treating wastewater containing heavy metal, such as Cu^{2+} and Pb^{2+}.

Introduction

Nowadays, heavy metals are one of the most important pollutants due to industrial and human activities (Shahnaz et al. 2016). Heavy metal contamination in industrial wastewater is a huge environmental problem because heavy metals cannot be metabolized and will constitute a great of threat to human health (Fu et al. 2011). Thus, appropriate techniques should be used to remove heavy metals from industrial wastewater before they are released into the environment. Several methods have been implemented to remove heavy metal, including membrane fifiltration, chemical precipitation, ion exchange, biological treatment, and adsorption. Among these methods, the adsorption method has the advantages of easy operation, high efficiency, good recyclability, and has been widely used (Bilal et al. 2013).

A variety of inorganic, organic, and organic/inorganic hybrid adsorbents have been developed to remove heavy metals from water treatment (Cui et al. 2015). However, many conventional adsorbents (e.g. activated carbon and clays) display inconvenient recyclability or expensive regeneration cost, and increase the expense for wastewater treatment. In recent years, biomass based materials have attracted extensive research and attention due to their advantages such as low cost, high absorption capacity, reproducibility and outstanding pollution control effect (Suhas et al. 2016; Kumar et al. 2017). As the main component of biomass based materials, cellulose has the advantages of being renewable (Nechyporchuk et al. 2016), biodegradaable and low cost (Denisov et al. 2017). Because it has a considerable number of hydroxyl groups, the oxygen in the hydroxyl group has unbonded electrons, which can cooperate with the vacant orbital of metal ions to form coordination bond adsorption, natural cellulose exhibits excellent adsorption properties for heavy metal (Wang et al. 2016).

However, the adsorption capacity of cellulose may not be as high as expected without any modification. In order to prepare cellulose based heavy metal ion adsorbents, the hydroxyl in cellulose must be modified by esterification, etherification and other chemical modifications (Gurgel et al. 2008). Although

many previous studies have focused on the modification of cellulose adsorbents, most of studies introduced functional groups directly on bulk cellulose (Aoki et al. 1999; Zhong et al. 2014; Ge et al. 2018; Godiya et al. 2019). In addition, only functional groups in the outer layer of cellulose fibers can be used, while a large number of hydroxyl groups are restricted by hydrogen bonds between cellulose microfibers. The organic solvent systems were required by these modification methods, which will harm the environment in some extent.

Previous studies reported that the surface of cellulose hydrogel after being oxidized by TEMPO (2,2,6,6-tetramethylpyperidine-1-oxy radical) tended to open holes (Lin et al. 2017; Saito 2010; Rodionova et al. 2012). The further modification of cellulose hydrogel is necessary to make it more competitive in practical application. Grafting branched polyethyleneimine (PEI) using glutaraldehyde crosslinking method has been reported to be an easy and cheap method of introducing amino groups on various materials with hydroxyl, aldehyde or carboxyl groups (Ma et al. 2014; Sun et al. 2011). By using glutaraldehyde crosslinking method, the adsorption capacity of the adsorbent can be greatly improved by grafting PEI. Therefore, in this paper, a highly functional heavy metal ion adsorbent was prepared by modifying oxidized cellulose hydrogel with PEI. The adsorbents were characterized by SEM, FTIR, XPS and elemental analyzer. Moreover, the effects of pH, adsorption time, initial ion concentration, temperature, coexisting ions concentration and competitive adsorption on cellulose hydrogel adsorption of Cu^{2+} and Pb^{2+} and performance were studied.

Materials And Methods

Materials and reagents

The polymerization degree of *poplar* cellulose was 534, preparing by the method of Lu (2014). Chemicals applied in this study were consist of 2,2,6,6-tetramethylpyperidine-1-oxy radical (TEMPO), polyethyleneimine (PEI, molecule weight of 1800 Da), glutaraldehyde, NaClO (0.9943 mol /L), $NaClO_2$, carbon tetrachloride (CCl_4), ethyl acetate, ice acetic acid. The urea ($CO(NH_2)_2$), $CuSO_4{\cdot}5H_2O$, $Pb(NO_3)_2$ were purchased from Aladdin Reagent Corp., China. Other reagents used in this work were of analytical grade and purchased from Xilong Chemical Co., Guangdong, China.

Preparation of the adsorbents

Poplar cellulose has poor solubility in NaOH/urea/water system with a high degree of polymerization. In this study, HCl/ethanol solution was used to pretreat the cellulose, and a lower degree of polymerization cellulose was obtained. At first, 50 g cellulose was hydrolyzed with 1 L hydrochloric acid/ethanol (HCl: ethanol = 1:25, V/V) at 70 ℃ for 2 h. Then, 4 g pretreated cellulose was hydrolyzed in 96 g NaOH/urea/water system solvent and stirred for 5 min. After cooled to -20 ℃ for 2 h, the solvent was stirred vigorously for 10 min, and resulting in a transparent solution. The solution was subjected to centrifugation for 20 min to remove air bubbles. In the following, 5 mL cellulose solution was absorbed by a disposable needle and dropped into the coagulation bath (trichloromethane: ethyl acetate: glacial

acetic acid = 3:3:1, V/V/V) to form hydrogel balls of the same size. After curing for 10 min, the hydrogel balls were placed in flowing water and washed to neutral. After that, the hydrogel balls were soaked in pure water for 3 days, and changed water every 6 h. The cellulose hydrogel balls named as CH.

0.5 g CH were taken into 50 mL 0.05 M pH = 6.8 phosphate buffer solution, which also contained 0.048 g TEMPO, 0.8475g $NaClO_2$ and 0.75 mL NaClO. The mixture was subjected in the McR-3 microwave chemical reactor at 60 ℃ for 6 h and the products was named as TCH. 1 g TEMPO-oxidized cellulose hydrogel (TCH) was added into 100 mL water and then PEI with different qualities (1, 2, 3 g) was added into TCH solution and stirred at 20 ℃ for 1 h. After that, 20 mL 1% glutaraldehyde solution was added dropwisely and reaction at 60 ℃ for 2 h. After three times of displacement in ethanol and tertiary butyl alcohol, PEI-modified poplar cellulose hydrogel were obtained after freeze-drying, and named as TCP.

Characterization

The morphologies of the hydrogels, were observed with the scanning electron microscopy (SEM, Hitachi S-4800, Japan) at an accelerating voltage of 3.0 kV. The functional groups of the hydrogels were characterized using a fourier transform infrared (FTIR) spectrometer (Bruker Tensor, Germany) within the wavenumber range of 500 cm^{-1}- 4000 cm^{-1}. The mass ratios of C, H and N of TCH and TCP were measured using elemental analyzer (Vario EL cube, Elementar Co., Germany). The C_{1s}, O_{1s} and N_{1s} spectra of adsorbents were characterized using a XPS instrument (ESCALAB 250Xi, Thermo-VG Scientific Co., US). Thermal properties of each absorbents were measured by thermogravimetry (TG 209, Germany). Heating was conducted under nitrogen with heating rate of 10 ℃/min from 35 ℃ to 700 ℃.

Adsorption experiments

Determination of carboxyl content

Carboxyl content of TCP was determined by conductivity titration. The TCP was ground into powder, and 0.3g TCP powder was added into 55 mL pure water with 5 mL 0.01mol/L NaCl. The mixture was stirred well and the pH of mixture was adjusted to 2.5-3.0 by HCL (0.1 mol/L). Finally, the mixture was titrated with 0.1 mol/L NaOH until the pH was 11, record the pH value during the titration. The carboxyl content can be calculated from the following Eqs.:

$$C_{COOH}=C*(V_2-V_1)/m$$

Where C is the concentration of NaOH (mol/L); V_1 is the volume of initial NaOH (L); V_2 is the volume of NaOH at the inflection point of the second derivative (L); m is the quality of sample.

Effect of adsorption time and pH on Cu^{2+} and Pb^{2+} adsorption

The adsorption kinetics of the TCP was evaluated by dosing 50 mg TCP into 50 mL 100 mg/L Cu^{2+} and Pb^{2+} solution. The pH of the Cu^{2+} solution and Pb^{2+} solution were controlled at 5.0. The mixture of the TCP and two ion solutions were shaken in a thermostatic shaker at 180 rpm and 30 ℃. At a

predetermined time intervals, the solution was collected and centrifuged. The Cu^{2+} and Pb^{2+} concentrations in the samples were examined using an ICP-AES (IRIS Intrepid IIXSP, Thermo Electron Corporation, USA). The influence of adsorption times (varying from 1 to 200 min) and pH (2–5) on the adsorption was examined. Because the high pH would cause the precipitation of Cu^{2+} and Pb^{2+}, the pH in this study was only set in the range 2–5.

In order to better perception of adsorption process, the kinetic predictions in the adsorption mechanism, as well as the controlling mechanism of adsorption process are remarkable and fundamental for the designation of adsorption equilibrium time and adsorption rate. Pseudo-first-order kinetics model, pseudo-second-order kinetics model and intraparticle diffusion (Xiao et al. 2017) were used to examine the adsorption kinetics, which can be expressed by Eqs. as following:

Pseudo-first-order kinetics model:

$$Q_t = Q_e(1-e^{-K1t})$$

pseudo-second-order kinetics model:

$$t/Q_t=1/(K_2\ Q_e^2) + t/Q_e$$

intraparticle diffusion:

$$Q_t = K_{id}t^{1/2}$$

Where Q_e is the equilibrium adsorption capacity (mg/g); Q_t is adsorption capacity (mg/g) at time t; t is adsorption time (min); K_1 is the pseudo first-order reaction rate constant (min^{-1}); K_2 is the pseudo-second-order reaction rate constant ($g{\cdot}mg^{-1}{\cdot}min^{-1}$); K_{id} is the intraparticle diffusion rate constant ($mg{\cdot}g^{-1}{\cdot}min^{-0.5}$). For pseudo-second-order kinetics model, when $t \rightarrow 0$, the initial

adsorption rate h could be defined as $h = k^2q_e^2$

Effect of initial Cu^{2+} and Pb^{2+} concentrations on adsorption

The adsorption isotherms of TCP was tested by dosing 30 mg TCP into flasks containing 50 mL Cu^{2+} and Pb^{2+} solution of different concentrations (50, 100, 150, 200, 250, 300, 350 and 400 mg/L). The mixture of adsorbent and two ion solutions were shaken in a thermostatic shaker at 180 rpm and 30 ℃ for 24 h to reach adsorption equilibrium.

Langmuir and Freundlich models were widely used to describe the adsorption process. The former wasvalid for monolayer sorption on the adsorbent surface with finite number of similar active sites, while the later was an empirical model which was valid for the multilayer adsorption. In this study, the two equilibrium models were used, which can be expressed by Eqs. as following (Charpentier et al. 2016):

Langmuir model:

$C_e/Q_e = C_e/Q_{max} + 1/(K_L Q_{max})$

Freundlich model:

$\log Q_e = \log K_F + 1/n (\log C_e)$

Where C_e is the concentration of Cu^{2+} at equilibrium (mg/L); Q_e is the adsorption of Cu^{2+} and Pb^{2+} at equilibrium (mg/g); Q_{max} is the maximum adsorption capacity (mg/g) at equilibrium; K_L is Langmuir adsorption constant (L/mg); K_F is Freundlich adsorption constant (mg/g); 1/n is the adsorption strength.The best-fit equilibrium model was determined based on the non-linear regression correlation coefficient (R^2).

Effect of temperature on Cu^{2+} and Pb^{2+} adsorption

The further study on the adsorption mechanism of TCP was tested by dosing 30 mg TCP into flasks containing 50 mL 100 mg/L Cu^{2+} and Pb^{2+} solution. The pH of the Cu^{2+} solution and Pb^{2+} solution were controlled at 5.0. The mixture of the TCP and two ion solutions were shaken in a thermostatic shaker at different temperatures (20, 30, 40, 50 ℃) and 180 rpm for 6h. Gibbs free energy (ΔG^o), adsorption heat or standard enthalpy (ΔH^o), and adsorption entropy (ΔS^o) of the thermodynamics parameters can be calculated from the following Eqs. (Sahmoune 2018):

$\Delta G^o = -RT \ln K_c$

$\ln K_c = \Delta S^o/R - \Delta H^o/(RT)$

$K_c = Q_e/C_e$

Where R, T, and K_c represent the gas constant (8.314 J mol^{-1} K^{-1}), Kelvin temperature and adsorption equilibrium constant, respectively; Q_e is the adsorption amount at equilibrium (mg/g); C_e is the concentration of Cu^{2+} and Pb^{2+} at adsorption equilibrium (mg/L).

Effect of coexisting ions on Cu^{2+} and Pb^{2+} adsorption

30 mg TCP was dosed into flasks containing 50 mL of 100 mg/L Cu^{2+} and Pb^{2+} solution with different ionic strengths. The pH of two ion solutions were controlled at 5.0. The mixture of the TCP and ion solutions were shaken in a thermostatic shaker at 180 rpm and 30 ℃ for 24 h to reach adsorption equilibrium. The concentration of Cu^{2+} and Pb^{2+} in the supernatant were determined after centrifuging to obtain the influence of different ionic strength on TCP adsorption. NaCl, KCl and $CaCl_2$ were selected as coexisting ions with 1.0, 2.0, 3.0, 4.0, 5.0 and 6.0 mmol.

The competitive adsorption of Cu^{2+} and Pb^{2+}

30 mg TCP was dosed into flasks containing 25 mL 50 mg/L Cu^{2+} and 25 mL 50 mg/L Pb^{2+} mixed solution. The pH of ion solution was controlled at 5.0. The mixture of the TCP and ion solution was shaken in a thermostatic shaker at 180 rpm and 30 ℃ for 24h to reach adsorption equilibrium. The concentration of Cu^{2+} and Pb^{2+} in the supernatant was determined after centrifuging to obtain the influence of competitive adsorption on TCP adsorption.

Desorption and regeneration experiments

In order to evaluate the stability of the adsorbent, the adsorption-desorption cyclic experiments were carried out. 30 mg freeze-dried TCP was dosed to 50 mL 100 mg/L Cu^{2+} and Pb^{2+} solution in a 250 mL flask, and were shaken in a thermostatic shaker at 180 rpm for 24 h. The pH of two ion solutions were controlled at 5.0. After the adsorption procedure completed, the TCP with Cu^{2+} or Pb^{2+} adsorbed was obtained by filtration and then regenerated with 100 mmol/L Na_2EDTA for 24 h to free the occupied adsorption sites. Then the regenerated adsorbents were rinsed several times with deionized water and dried at ambient temperature. The air-dried adsorbent was added in 100 mg/L Cu^{2+} and Pb^{2+} solution again for the next adsorption experiment. The adsorption-desorption experiment was carried out in 5 cycles in total and the adsorption capacity of TCP in each cycle was measured.

Results And Discussion

Characterization of TCP absorbent

The surface and cross-section morphologies of CH, TCH and TCP were shown in Fig. 1. It can be seen that the surface of the CH was flat. After TEMPO oxidization, the typical network structure was occurred. After grafted with PEI, a PEI layer covered uniformly around the TCP which forming quantities of pores with small size between the TCP branches. The specific surface area of TCP was increased by the grafting of PEI and thus the accessibility of metal ions to the TCP would be promoted. The FTIR spectra of CH (a), TCH (b) and TCP (c) were presented in Fig. 2. The peaks at 3409 cm^{-1} and 2900 cm^{-1} were attributed to the tensile vibration of O-H and C-H, respectively (Zhang et al. 2016). The band at 1112 cm^{-1} was assigned to the stretching vibration of C-O, and the 1638 cm^{-1} was the characteristic peak of cellulose water absorption (Zhang et al. 2016). New absorption peaks at 1614 cm^{-1} and 1415 cm^{-1} were appeared after TEMPO oxidization, which belonged to -COO- (Lin et al. 2017). This results showed that carboxyl were successfully introduced into CH after TEMPO oxidization. Due to the superposition of O-H and N-H absorption peaks, the absorption peak of TCH (Fig. 2b) at 3422 cm^{-1} became broad in Fig. 2c. The stretching vibrations of N-H at 1613 cm^{-1} and C-N stretching vibrations at 1456 cm^{-1} in TCP spectrum also proved the successfully introduction of PEI to oxidized cellulose hydrogel (Zhang et al. 2016; Guo et al. 2017).

The contents of C, N and H in different cellulose-based adsorbents were listed in Table 1. The N content of oxidized cellulose was increased significantly after the reaction with PEI, indicating that PEI was successfully introduced into TCH. Due to the high content of N element in PEI, the N content of TCP was

increased significantly from 0.016–11.574% (TCH: PEI = 1:1) compared to that of oxidized cellulose. The N content of TCP tended to be stable with the addition of PEI, indicating that the amount of PEI was overused during the reaction. The contents of each element in TCP was presented in Fig. 3, TCP was mainly composed of C (67.04 %), N (13.69 %), O (19.27 %). The peak fitting of C_{1s}, O_{1s} and N_{1s} showed that C-C (284.7eV), C-N (285.4 eV), C-O (285.9 eV), and C = O (287.4 eV) bonds were existed in TCP. The three fitting peaks of N_{1s} in TCP were primary amine (398.51eV), secondary amine (399.18eV), and tertiary amine (400.7eV), respectively (Zhao et al. 2017). The results of elemental analysis data, the XPS and FTIR spectra confirmed that PEI was grafted successfully on TCH.

Table 1
Elemental analysis of TCH and TCP

	C (%)	H (%)	N (%)
TCH	38.758	5.795	0.016
TCH: PEI (1:1)	47.905	7.443	11.574
TCH: PEI (1:2)	47.035	7.760	11.141
TCH: PEI (1:3)	46.497	7.755	11.232

The thermal stabilities of CH, TCH and TCP were determined by thermogravimetric analysis in nitrogen from 35 ℃ to 700 ℃ (Fig. 4). Due to the carbonization and pyrolysis of cellulose, the main pyrolysis interval of *poplar* cellulose appeared at 338 ℃-375 ℃, and the mass loss at this stage was 77.46%. Compared with poplar cellulose, the initial pyrolysis temperature of oxidized cellulose was at 222.8 ℃. This phenomenon was mainly due to the decrease of crystallinity of oxidized cellulose (Yang 2011), and the initial decomposition temperature could be advanced by the presence of carboxyl (Zhao et al. 2017). The thermal decomposition peaks of 173–195 ℃ and 343–385 ℃ appeared in TCP (Zhao et al. 2017; Li et al. 2018) was due to the aminolysis of PEI and the broke of PEI chain. In addition, the final residual masses of oxidized cellulose and TCP were 28.36% and 15.78%, indicating that the thermal stability of TCP was reduced.

Effect of oxidation time on the carboxyl content and adsorption amount of TCP were shown in Fig. 5. The oxidation process of CH can be accelerated by microwave. The carboxyl content of CH increased rapidly with the increase of oxidation time, which was consistent with Lin's (Lin et al. 2017) study. The cuticle of CH was peeled off, and the carboxyl content was increased by the process of oxidation, which provided a large number of adsorption sites for Cu^{2+}. The adsorption capacity of TCP on Cu^{2+} was also increased with the increase of oxidation time, and the carboxyl content and adsorption capacity reached the maximum at oxidation time of 6 h. Therefore, the hydrogels with oxidation time of 6 h were selected for further experiments. The adsorption amount of TCH was increased significantly after grafted with PEI, while the adsorption amount was limited increased with the increase of PEI. Finally, TCH: PEI = 1:1 was selected as the research object in this study.

Adsorption performance

Effect of pH on Cu^{2+} and Pb^{2+} adsorption

The effect of pH value on the adsorption capacity of heavy metals is one of important parameters for sorption process. The pH dependence of metal adsorption is closely related to the surface functional groups of the adsorbent (Dehghani et al. 2016). The adsorptions of Cu^{2+} and Pb^{2+} by TCP at various pH values were shown in Fig. 6 (pH value in solution was 2–5). TCP adsorption capacities of Cu^{2+} and Pb^{2+} were gradually increased with the increase of pH value. At solution pH = 2, the TCP adsorption capacities of Cu^{2+} and Pb^{2+} were 15.02 mg/g and 24.18 mg/g, respectively. At pH = 5, TCP adsorption capacities of Cu^{2+} and Pb^{2+} were increased to 104.44 mg/g and 123.76 mg/g, respectively. At low pH values, a large number of H^{+} competed with Cu^{2+} and Pb^{2+} for adsorption sites, resulting in extremely low adsorption capacity of TCP (Niu et al. 2017). At higher pH values, deprotonated functional groups (amino) could chelation with Cu^{2+} and Pb^{2+}. Besides, electrostatic forces between adsorbent and heavy metal ions were also increased, resulting in the sharply increasing of adsorption capacity of TCP. Therefore, the pH of the solution was adjusted to 5 in the subsequent experiments.

Effect of adsorption time on Cu^{2+} and Pb^{2+} adsorption

The effect of different adsorption time on Cu^{2+} and Pb^{2+} adsorption was shown in Fig. 7. As shown in Fig. 7a, the adsorption of Cu^{2+} and Pb^{2+} by TCP reached saturation in 45 min. In the initial stage of adsorption, there were a large number of active adsorption sites (amino, carboxyl, and hydroxyl) on the TCP, the adsorption rate were fast. With the increase of the adsorption time, the concentrations of Cu^{2+} and Pb^{2+} were decreased, and the active adsorption sites were occupied by Cu^{2+} and Pb^{2+}. The concentration difference between the metal ions and TCP decreased, resulting the decrease of adsorption rate until the adsorption equilibrium (Gao et al. 2016).

Pseudo-first-order kinetics model, pseudo-second-order kinetics model, and intraparticle diffusion were used to investigate adsorption kinetic mechanisms (Xiao et al. 2017). The simulated curves of Cu^{2+} and Pb^{2+} adsorption by TCP were shown in Fig. 7, and the fitting parameters were shown in Table 2. It can be seen that the adsorption process of Cu^{2+} and Pb^{2+} fitted well by pseudo-second-order kinetics, and the adsorption amounts obtained by fitting were close to the actual measured results. Pseudo-second-order kinetics results showed that TCP adsorption was controlled by chemisorption. As shown in Fig. 7b, the adsorption processes of Cu^{2+} and Pb^{2+} by TCP were divided into two stages. Firstly, the amino and carboxyl groups on TCP rapidly chelating to Cu^{2+} and Pb^{2+}, which were controlled by chemical adsorption. Then, Cu^{2+} and Pb^{2+} were adsorbed slowly into the TCP and controlled by intraparticle diffusion. Although TCP had similar adsorption processes for Cu^{2+} and Pb^{2+}, the Pb^{2+} adsorption rate of TCP was higher than that of Cu^{2+}.

Table 2
Adsorption kinetics and intraparticle diffusion model parameters for the adsorption of Cu^{2+} and Pb^{2+} by TCP

		Cu^{2+}	Pb^{2+}
pseudo-first-order kinetics model	Q_e(mg·g^{-1})	97.6857	128.3174
	K_1 (min^{-1})	0.0973	0.0915
	R^2	0.9940	0.9918
pseudo-second-order kinetics model	Q_e(mg·g^{-1})	103.3058	136.2398
	K_2(g·mg^{-1}·min^{-1})	0.0019	0.0014
	R^2	0.9996	0.9998
intraparticle diffusion model	$k_{i,1}$(mg·g^{-1}·min$^{-0.5}$)	6.3494	8.8439
	$k_{i,2}$(mg·g^{-1}·min$^{-0.5}$)	0.9983	0.9242

Effect of initial Cu^{2+} and Pb^{2+} concentrations on adsorption

Initial concentrations of the heavy metal ions play a major role in the adsorption capacity. Generally, the influence of initial metal ions concentration rely on the relative between the existing sites on an adsorbent surface and concentration of the heavy metals (Geng et al. 2017). The relationship between adsorbents and adsorbates can be revealed by the adsorption isotherm (Guo et al. 2017). The effects of different initial Cu^{2+} and Pb^{2+} concentrations on adsorption were shown in Fig. 8a. With the increase of initial Cu^{2+} and Pb^{2+} concentrations, the adsorption of Cu^{2+} and Pb^{2+} by TCP showed gradually increasing trend, and the adsorption capacity of Pb^{2+} was higher than that of Cu^{2+}. When the initial concentrations were greater than 300 mg/L, adsorption of Cu^{2+} and Pb^{2+} by TCP reached saturation, and the adsorption capacity was stable. Langmuir and Freundlich models were used to investigate the adsorption mechanism. The Langmuir model assumed that the adsorbent surface had a finite number of binding sites with the same energy, and each binding site absorbed a single ion (Charpentier et al. 2016). The Freundlich model assumed that different binding sites on the adsorbent surface was based on multimolecular layer adsorption (Lin et al. 2017). The adsorption isotherms of the Langmuir and Freundlich models were shown in Fig. 8b and Fig. 8c. Adsorption isotherm parameters for the adsorption Cu^{2+} and Pb^{2+} by TCP were shown in Table 3. As shown in Table 3, the adsorption processes of TCP could be well fitted by the Langmuir model, and the fitting coefficients were all greater than 0.999. The actual adsorption capacities of TCP were consistent with the fitted maximum adsorption capacity. The isothermal adsorption conformed to the Langmuir model, indicating that the adsorptions of Cu^{2+} and

Pb^{2+} by TCP were belonged to the single molecular layer adsorption. According to the Langmuir model, the maximum adsorption capacity of Cu^{2+} and Pb^{2+} by TCP was 109.89 mg/g and 279.33 mg/g, respectively, which were far higher than other cellulose-based adsorbents (Table 4). This results might due to that TCP had large number of active chelate functional groups (amino, carboxyl, hydroxyl) and pore structures, it could provided many adsorption sites for heavy metal ions.

Table 3
Adsorption isotherm parameters for the adsorption Cu^{2+} and Pb^{2+} by TCP

	Langmuir			**Freundlich**		
	Q_{max} (mg·g^{-1})	K_L (L/mg)	R_L^2	K_F (mg·g^{-1})	n	R_F^2
Cu^{2+}	109.8901	0.1569	0.9993	56.7819	8.3998	0.8139
Pb^{2+}	279.3296	0.0868	0.9991	66.7882	3.6426	0.9009

Table 4
Comparison of adsorption capacities of various adsorbents for the adsorption of Cu^{2+} and Pb^{2+} from the aqueous solution

Adsorbents	**The adsorption capacity (mg/g)**		
	Cu^{2+}	**Pb^{2+}**	**Ref.**
PEI-modified TEMPO oxidized nano-cellulose aerogel	52.32	-	(Zhang et al. 2016)
Guanyl-modified cellulose aerogel	83	52	(Kenawy et al. 2018)
Succinic anhydride modified mercerized cellulose aerogel	30.4	205.9	(Gurgel et al. 2008)
Glycidyl methacrylate cellulose aerogle	70.4	84.87	(Hokkanen et al. 2016)
CSTEC	95.24	144.93	(Niu et al. 2017)
TCP	109.89	279.33	This study

Effect of temperature on Cu^{2+} and Pb^{2+} adsorption

Temperature is another major parameter to influence the adsorption property. The adsorption capacity was effected by temperature which could change the molecular interactions and solubility. The effect of different temperatures on Cu^{2+} and Pb^{2+} adsorption by TCP were shown in Fig. 9. With the increase of temperature, the adsorptions of Cu^{2+} and Pb^{2+} by TCP were both gradually increased, indicating that the adsorptions were endothermic process (Dehghani et al. 2016). The adsorption mechanism was analyzed

by linear fitting of thermodynamic parameters (ΔG^o, ΔH^o, and ΔS^o), and the results were shown in Table 5. Negative value of ΔG^o indicated that the adsorption process was spontaneous, and temperature was advantageous to the adsorption process. Positive value of ΔH^o and ΔS^o indicated that the adsorption process was endothermic, and the randomness of the solid-liquid interface was increased during the adsorption process (Demiral et al. 2016).

Table 5
Adsorption thermodynamics parameters for the adsorption of Cu^{2+} and Pb^{2+} by TCP

	ΔG^o (KJ/mol)				ΔH^o (KJ/mol)	ΔS^o (J/mol/K)	R^2
	293 K	303 K	313 K	323K			
Cu^{2+}	-1.3012	-1.5118	-1.7223	-1.9328	4.8678	21.0546	0.9979
Pb^{2+}	-5.0854	-5.6214	-6.1572	-6.6932	10.6165	53.5904	0.9992

Effect of coexisting ions on Cu^{2+} adsorption

The actual pollutants commonly include various heavy metal ions and other coexistent ions such as Cl^-, NO^{3-}, SO_4^{2-}, PO_4^{3-}, which might affect the adsorption capacity of target pollutant (Guo et al. 2018). However, it is precisely the existence of coexisting ions that can cause an inhibition for the adsorption process of heavy metal ions. The morphology of heavy metals and the adsorption sites of adsorbents could be affected by coexisting ions (Wang et al. 2019). The effect of coexisting ions on Cu^{2+} adsorption were discussed in this study, and the results were shown in Fig. 10. TCP had a small adsorption capacity for Cu^{2+} at low $NaNO_3$ concentration (below 1 M). While $NaNO_3$ concentration was 1 M, the adsorption of Cu^{2+} by TCP decreased slightly from 103 mg/g to 99 mg/g. Because of the activity coefficient of Cu^{2+} could be affected by high ion concentration, TCP adsorption capacity for Cu^{2+} was declined at high ion concentration. The results showed that the coexisting ions had little effect on the adsorption of Cu^{2+} by TCP.

The competitive adsorption of Cu^{2+} and Pb^{2+}

In the natural environment, Cu^{2+} and Pb^{2+} often coexist in contaminated areas. The influence of single system and coexistence system on TCP adsorption were shown in Fig. 11. The adsorption capacities of Cu^{2+} and Pb^{2+} by TCP in the single system were 65.23 mg/g and 78.81 mg/g, respectively. In the coexistence system (Cu^{2+} and Pb^{2+}), the adsorption capacity of Cu^{2+} was slightly decreased to 64.42 mg/g, while that of Pb^{2+} significantly decreased to 52.03 mg/g. Because TCP had a higher affinity for Cu^{2+} than Pb^{2+}, Cu^{2+} could compete with Pb^{2+} for adsorption sites.

Recycling performance of TCP

Recycling stability is also a significant factor for an adsorbent in the practical application. In order to evaluate the regeneration ability of TCP, 100 mmol/L Na_2EDTA was used to desorb Cu^{2+} and Pb^{2+} from the adsorbent. Figure 12 showed the performance of TCP for Cu^{2+} and Pb^{2+} adsorption during 5 adsorption-desorption cycles. The results showed that the adsorption capacities of Cu^{2+} and Pb^{2+} by TCP were decreased with the increase of cycle times. In the second cycle, the Cu^{2+} and Pb^{2+} adsorption quantity was 77.28 mg/g and 116.94 mg/g, respectively. The decrease of adsorption capacity in the second cycle might be due to that some active sites of the absorbent combined with metal ions in an irreversible way, reducing the density of ions binding sites in the second cycle. Obviously, TCP still had a high adsorption capacity for Cu^{2+} and Pb^{2+} after 5 cycles with an adsorption capacity of 58.26 mg/g for Cu^{2+} and 91.96 mg/g for Pb^{2+}. Although the adsorption capacity of the regenerated TCP was far lower than that of the original TCP, it still had a good adsorption effect. The stability in the adsorption-desorption experiment implied that the good regeneration ability of TCP, making it a practical adsorbent in the real wastewater treatment.

Adsorption mechanism

The functional groups change for the adsorption of Cu^{2+} and Pb^{2+} by TCP were shown in Fig. 13. The absorption peaks were belonged to amino, and the peak of hydroxyl at 3422 cm^{-1} became weaker after adsorption. This peak was shifted to 3432 cm^{-1} and 3440 cm^{-1} after adsorption of Cu^{2+} and Pb^{2+}, respectively, indicating that the amino and hydroxyl in TCP were involved in Cu^{2+} and Pb^{2+} adsorption. In addition, the absorption peaks belonged to N-H and C-N at 1613 cm^{-1} and 1456 cm^{-1} were also changed after adsorption. The results of XPS spectrum further confirmed the adsorption mechanism (Fig. 14). After adsorption, the absorption peaks of Cu_{2p} at 933.86 eV and Pb_{4f} at 138.16 eV were appeared (Lin et al. 2017), indicating the successful adsorption of Cu^{2+} and Pb^{2+} by the TCP. Meanwhile, the absorption peaks belonged to -NH_2 were shifted from 398.51eV to 399.22 eV and 398.82 eV, respectively, and the peaks belonged to -NH- were shifted from 399.15 eV to 399.96 eV and 399.85 eV, respectively. Furthermore, the peaks belonged to -N- were shifted from 400.7 eV to 400.98 eV and 401.33 eV, respectively. All of peaks were shifted to higher binding energies, indicating that primary, secondary and tertiary amines were played an important role in the adsorption. Moreover, a new absorption peak appeared at 406.49 eV in N_{1s} after the adsorption of Pb^{2+}, probably due to the formation of compound between N and Pb^{2+} on the primary and secondary amino groups. This result was consistent with the study of Zhao (Zhao et al. 2017). The above results confirmed that the hydroxyl, amino and carboxyl groups on the surface of TCP played an important role in the adsorption.

Conclusion

In this study, a *poplar* cellulose based adsorbent for Cu^{2+} and Pb^{2+} uptake was prepared. Further characterization confirmed that large amounts of carboxyl groups

and amino groups had been successfully introduced to the adsorbent. The maximum adsorption capacity of Cu^{2+} and Pb^{2+} by TCP was 109.89 mg/g and 279.32 mg/g, respectively, which were significantly higher than cellulose-based adsorbents in other studies. Langmuir model fitted the adsorption process well and showed that TCP was a single molecule adsorption process. Adsorption kinetics showed that the Pb^{2+} adsorption rate of TCP was higher than that for Cu^{2+}. The coexisting ion contents had little influence on the adsorption of Cu^{2+} by TCP. Because TCP had a higher affinity for Cu^{2+} than Pb^{2+}, Cu^{2+} could compete with Pb^{2+} for adsorption sites. After 5 cycles, the adsorption capacity of TCP for Cu^{2+} and Pb^{2+} was 58.26 mg/g and 91.96 mg/g, respectively. Considering the ultra-porosity structure, green synthetic way, recyclable and supreme adsorption, the TCP as a native adsorbent can be compete as appropriate candidate for the treatment of effluent polluted with heavy metal ions.

Declarations

Acknowledgments This work was supported by the Anhui Science Foundation Grant (1808085MC68); University Natural Science Research of Anhui Education Ministry (KJ2016A833); Anhui Postdoctoral Science Foundation Grant (2017B157); 13th Five-Year National Major Research and Development Program Sub-topic (2017YFD0600201).

Conflicts of interest The authors have no conflicts of interest to declare that are relevant to the content of this article.

Human or animal rights The work described in this article did not involve human participants and or animals.

Authors controbutions Xinyi Xing: Writing and Editing · Wenqi Li: Data curation, Writing- Original draft preparation · Jie Zhang: Article revision · Han Wu: Supervision · Ying Guan: Conceptualization · Hui Gao: Methodology

References

Aoki N, Fukushima K, Kurakata H (1999) 6-Dexoy-6-mercaptocellulose and its S-substituted derivatives as sorbents for metal ions. React Funct Polym 42:223-233.

Bilal M, Shah JA, Ashfaq T, Gardazi SMH, Tahir AA, Pervez A (2013) Waste biomass adsorbents for copper removal from industrial wastewater—A review. J. Hazard Mater 263:322-333.

Charpentier TVJ, Neville A, Lanigan JL, Barker RJ, Richardson T (2016) Preparation of magnetic carboxymethylchitosan nanoparticles for adsorption of heavy metal ions. ACS Omega 1:77-83.

Cui L, Wang Y, Gao L, Hu L, Yan L, Wei Q, Du B (2015) EDTA functionalized magnetic graphene oxide for removal of Pb(II), Hg(II) and Cu(II) in water treatment: adsorption mechanism and separation property. Chem.Eng.J 281:1-10.

Dehghani MH, Sanaei D, Ali I (2016) Removal of chromium(VI) from aqueous solution using treated waste newspaper as a low-cost adsorbent: Kinetic modeling and isotherm studies. J. Mol. Liq 215:671-679.

Demiral H, Güngör C (2016) Adsorption of copper(II) from aqueous solutions on activated carbon prepared from grape bagasse. J. Clean. Prod 124:103-113.

Denisov IG, Sligar SG (2017) Nanodiscs in Membrane Biochemistry and Biophysics. Chem. Rev 117:4669-4713.

Fu F, Wang Q (2011) Removal of heavy metal ions from wastewaters: a review. J. Environ. Manage 92:407-418.

Gao ZM, Jiang JH, Luo CW, Ren HX, Wu DJ (2016) Efficient Pb(II) removal using sodium alginate-carboxymethyl cellulose gel beads: Preparation, characterization, and adsorption mechanism. Carbohydr. Polym 137:402-409.

Ge, Xuesong, Youna, Shan (2018) High-strength and morphology-controlled aerogel based on carboxymethyl cellulose and graphene oxide. Carbohydr. Polym 197:277–283.

Geng B, Wang H, Shuai W, Jing R, Liu XY (2017) Surface-tailored nanocellulose aerogels with thiol-functional moieties for highly efficient and selective removal of Hg (II) ions from water. ACS Sustain Chem Eng 5:11715-26

Godiya B, Liang M, Mir Sayed V, D. Li, Lu X (2019) Novel lginate / polyethyleneimine hydrogel adsorbent for cascaded removal and utilization of Cu2+ and Pb2+ ions. Environ Manage 232:829–841.

Guo DM, An QD, Xiao ZY, Zhai SR, Shi Z (2017) Polyethylenimine-functionalized cellulose aerogel beads for efficient dynamic removal of chromium(vi) from aqueous solution. RCS Adv 7:54039-54052.

Guo DM, An QD, Xiao ZY, Zhai SR, Yang DJ (2018) Efficient removal of Pb(II), Cr(VI) and organic dyes by polydopamine modified chitosan aerogels. Carbohydr. Polym 202:306-14.

Gurgel LVA, Júnior OK, Gil RPDF (2008) Adsorption of Cu(II), Cd(II), and Pb(II) from aqueous single metal solutions by cellulose and mercerized cellulose chemically modified with succinic anhydride. Bioresour. Technol 99:3077-3083.

Hokkanen S, Bhatnagar A, Sillanpaa M (2016) A review on modification methods to cellulose-based adsorbents to improve adsorption capacity. W*ater* Res 91:156-173.

Kenawy IM, Hafez MAH, Ismail MA, Hashem MA (2018) Adsorption of Cu(II), Cd(II), Hg(II), Pb(II) and Zn(II) from aqueous single metal solutions by guanyl-modified cellulose. Int J Biol Macromol 107:1538-1549.

Kumar R, Sharma RK, Singh AP (2017) Cellulose based grafted biosorbents - Journey from lignocellulose biomass to toxic metal ions sorption applications - A review. J. Mol. Liq 232:62-93.

Li J, Zuo KM, Wu WM, Xu ZY, Yi YG (2018) Shape memory aerogels from nanocellulose and polyethyleneimine as a novel adsorbent for removal of Cu(II) and Pb(II). Carbohydr. Polym 196:376-384.

Lin F, You Y, Yang X, Jiang X, Lu B (2017) Microwave-assisted facile synthesis of TEMPO-oxidized cellulose beads with high adsorption capacity for organic dyes. Cellulose 24:5025-5040.

Lin Y, Hong Y, Song Q, Zhang Z, Gao J, Tao T (2017) Highly efficient removal of copper ions from water using poly(acrylic acid)-grafted chitosan adsorbent. *Colloid* Polym Sci 295:627-635.

Lu YJ (2014) A comparison of the performance of the regenerated cellulose film of Zhonglin-46 poplar normal wood and tension wood. Doctoral dissertation.

Ma Y, Liu WJ, Zhang N, Li YS, Jiang H, Sheng GP (2014) Polyethylenimine modified biochar adsorbent for hexavalent chromium removal from the aqueous solution. Bioresour. Technol 169:403-408.

Nechyporchuk O, Belgacem MN, Bras J (2016) Production of cellulose nanofibrils: A review of recent advances. *Ind Crops Prod* 93:2-25.

Niu Y, Li K, Ying D, Wang Y, Jia J (2017) Novel recyclable adsorbent for the removal of copper(II) and lead(II) from aqueous solution. Bioresour. Technol 229:63-68.

Rodionova G, Oyvind Eriksen, Oyvind Gregersen (2012) TEMPO-oxidized cellulose nanofiber films: effect of surface morphology on water resistance. Cellulose 19:1115-1123.

Sahmoune MN (2018) Evaluation of thermodynamic parameters for adsorption of heavy metals by green adsorbents. Environ Chem Lett 1-8.

Saito T (2010) Structural analysis of TEMPO-oxidized Cellulose Nanofibers. Fiber 66.

Shahnaz K, Jafari P, Rabiei J, Irani M, Aliabadi M (2016) Fabrication of PET/PAN/GO/Fe3O4 nanofibrous membrane for the removal of Pb(II) and Cr(VI) ions. Chem. Eng.J 301:42-50.

Suhas, Gupta VK, Carrott PJ, Singh R, Chaudhary M, Kushwaha S (2016) Cellulose: A review as natural, modified and activated carbon adsorbent. Bioresour. Technol 216:1066-1076.

Sun XF, Wang SG, Cheng W, Fan M, Tian BH, Gao BY (2011) Enhancement of acidic dye biosorption capacity on poly(ethylenimine) grafted anaerobic granular sludge. J. *Hazard* Mater 189:27-33.

Wang LY, Wang MJ (2016) Removal of heavy metal ions by poly (vinyl alcohol) and carboxymethyl cellulose composite hydrogels prepared by a freeze-thaw method. *ACS* Sustain. Chem. Eng 2830-2837.

Wang XL, Guo DM, An QD, Xiao ZY, Zhai SR (2019) High-efficacy adsorption of Cr(VI) and anionic dyes onto β-cyclodextrin/chitosan/hexamethylenetetramine aerogel beads with task-specific, integrated components. Int J Biol Macromol 128:268-78.

Xiao C, Liu X, Mao S, Zhang LJ, Lu J (2017) Sub-micron-sized polyethylenimine-modified polystyrene/ Fe_3O_4 /chitosan magnetic composites for the efficient and recyclable adsorption of Cu(II) ions. Appl. Surf. Sci 394:378-385.

Yang JX (2011) Oxidized cellulose nanofibers were prepared by TEMPO oxidation method. J Nor For Univ 39:96-98.

Zhang N, Zang GL, Shi C, Yu HQ, Sheng GP (2016) A novel adsorbent TEMPO-mediated oxidized cellulose nanofibrils modified with PEI: Preparation, characterization, and application for Cu(II) removal. J. *Hazard* Mater 316:11-18.

Zhao F, Repo E, Song Y (2017) Polyethylenimine-cross-linked cellulose nanocrystals for highly efficient recovery of rare earth elements from water and a mechanism study. Green Chem 19:4816-4828.

Zhong QQ, Yue QY, Li Q, Gao BY, Xu X (2014) Removal of Cu(II) and Cr(VI) from wastewater by an amphoteric sorbent based on cellulose-rich biomass. Carbohydr. Polym 111:788-796.

Figures

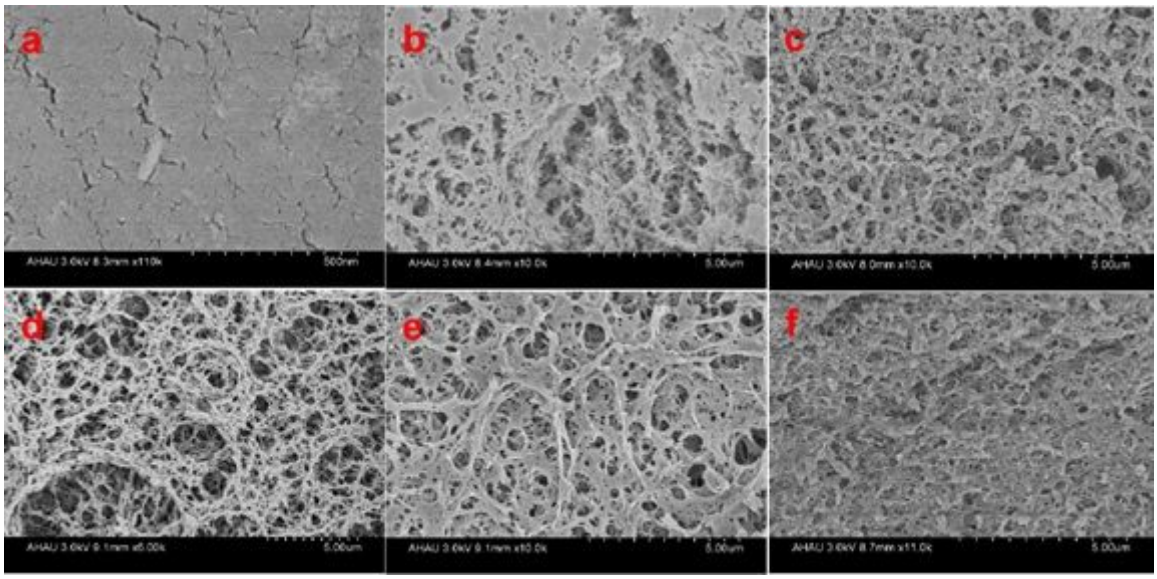

Figure 1

SEM images of the surface and cross-section morphologies of CH (a and d), TCH (b and e), and TCP (c and f).

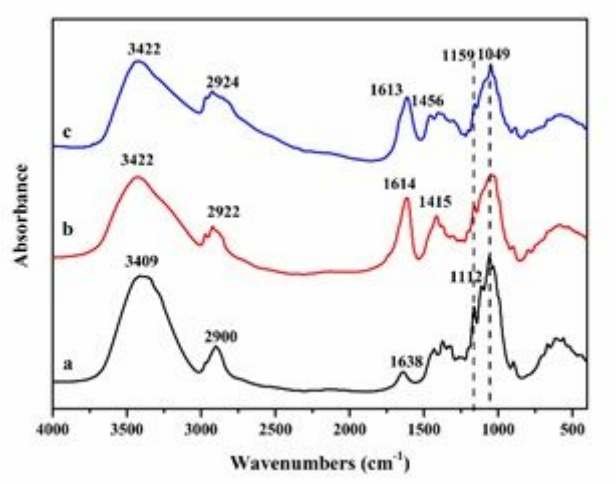

Figure 2

FTIR spectra of (a) CH, (b) TCH, and (c) TCP.

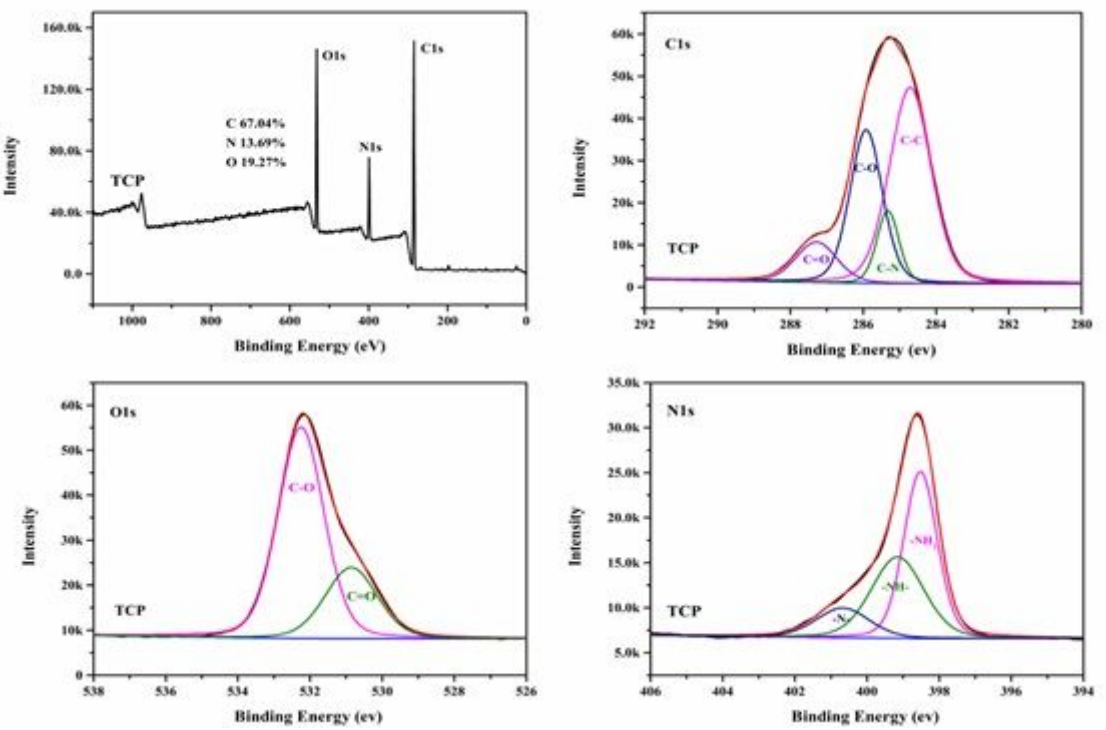

Figure 3

The wide XPS spectra and high-resolution XPS spectra of C1s, O1s , and N1s in TCP.

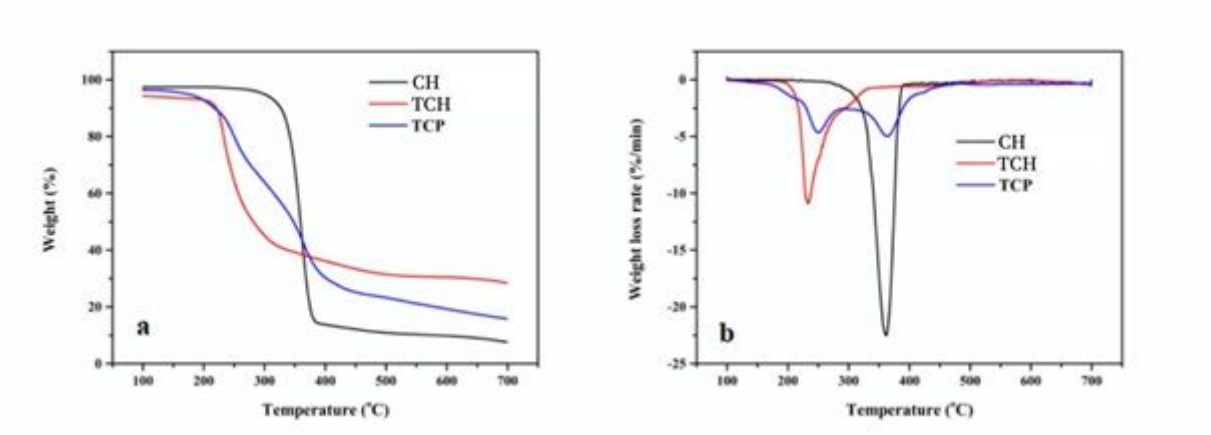

Figure 4

TG (a) and DTG (b) spectra of CH, TCH, and TCP.

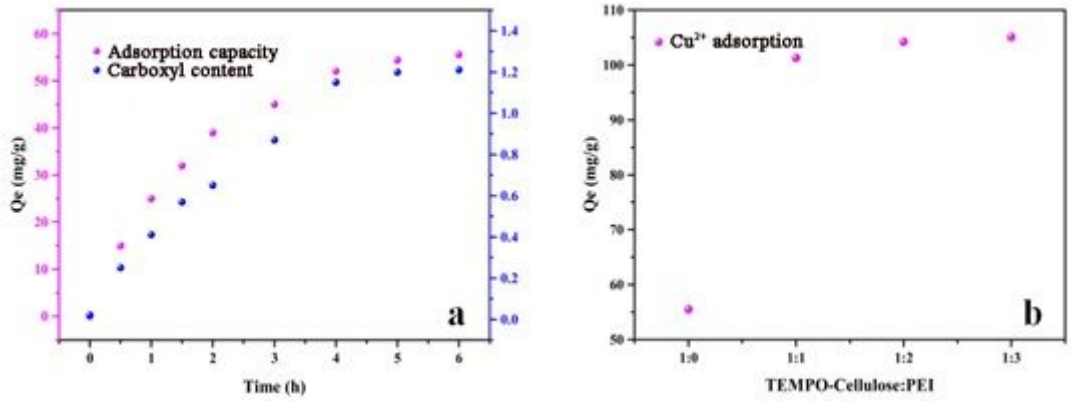

Figure 5

Effect of oxidation time on the carboxyl content and adsorption amount of TCP (a), effect of PEI content on the adsorption amount (b).

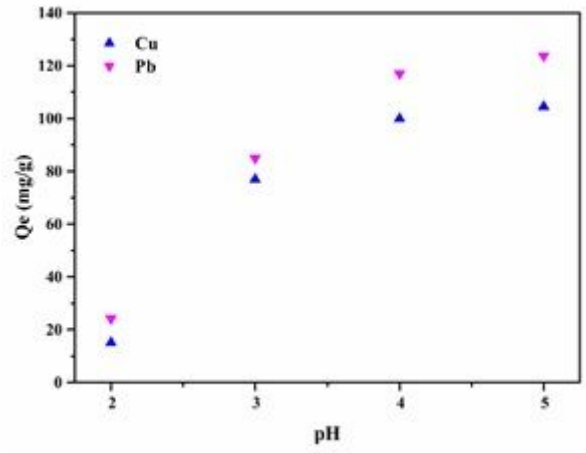

Figure 6

The adsorptions of Cu2+ and Pb2+ by TCP at various pH values.

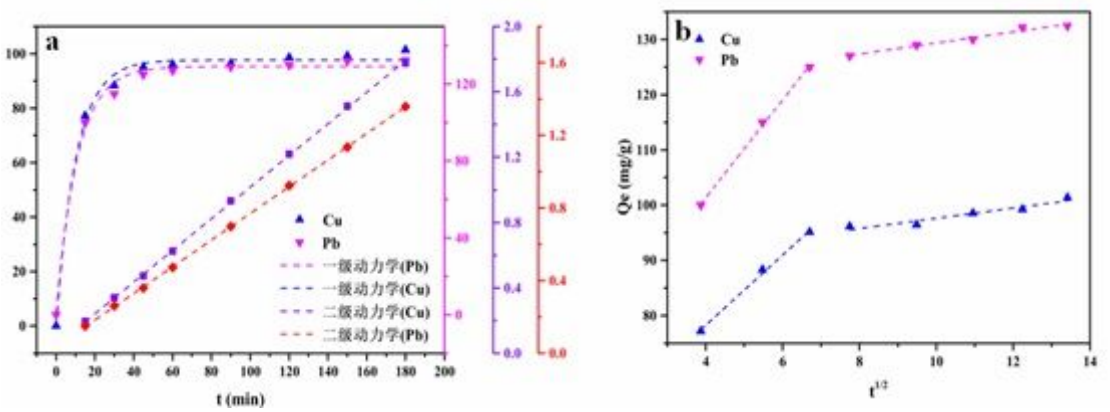

Figure 7

The adsorption kinetics of Cu2+ and Pb2+ adsorption by TCP (a: linear plot of pseudo-first-order and pseudo-second-order; b: Intraparticle diffusion model).

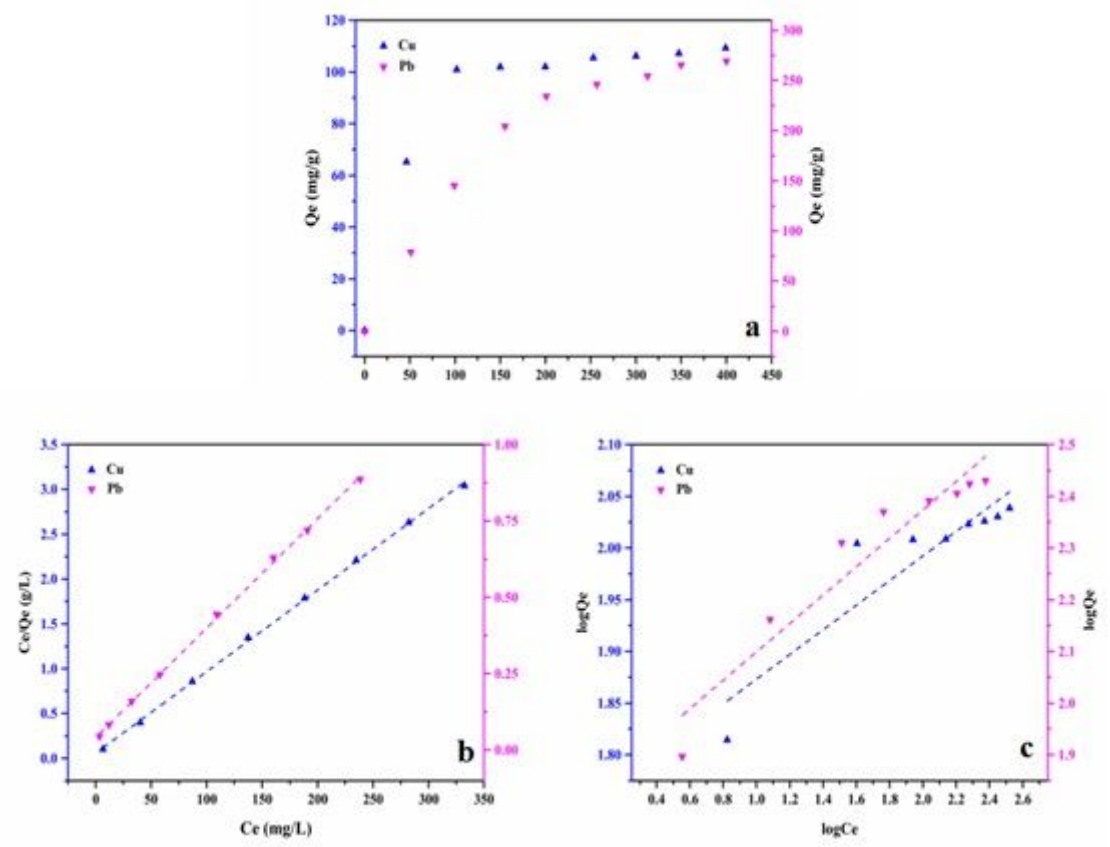

Figure 8

The effects of different initial Cu2+ and Pb2+ concentrations on adsorption (a) and the adsorption isotherms of the Langmuir (b) and Freundlich (c) models.

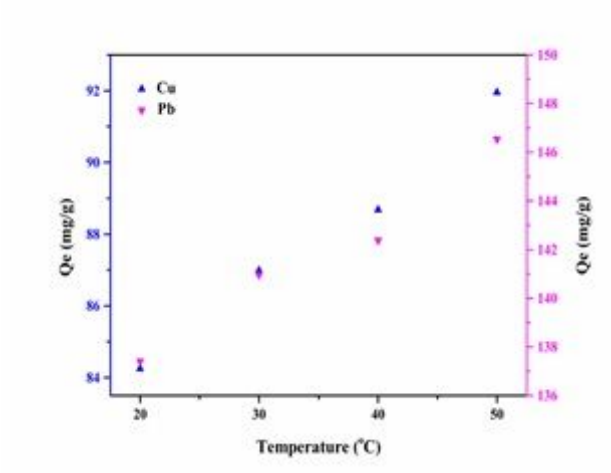

Figure 9

The effect of different temperatures on Cu2+ and Pb2+ adsorption by TCP.

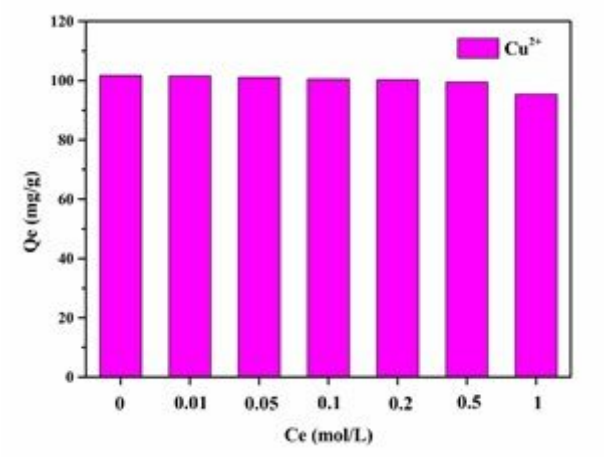

Figure 10

The effect of the ionic strength (NaNO3) on the adsorption Cu2+.

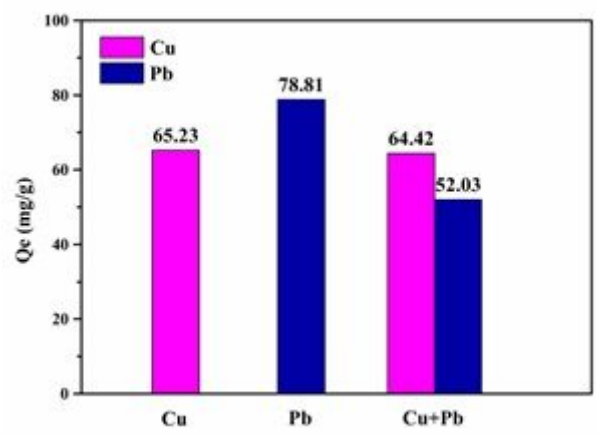

Figure 11

Adsorption of Cu2+ and Pb2+ from single and binary mixtures.

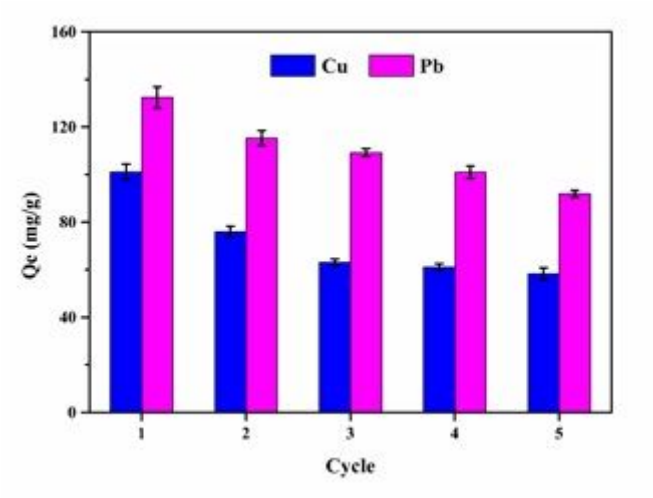

Figure 12

Recycling stability of TCP for the adsorption of Cu2+ and Pb2+.

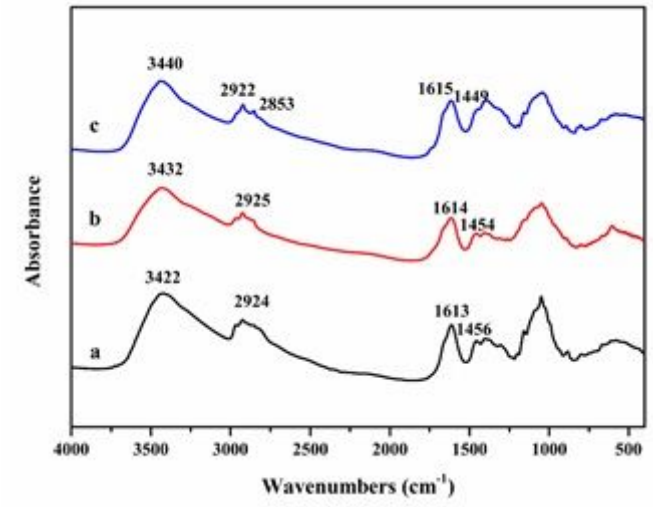

Figure 13

FTIR spectra of TCP before and after adsorption of Cu2+ and Pb2+ (a: before adsorption, b: after adsorption of Cu2+, c: after adsorption of Pb2+).

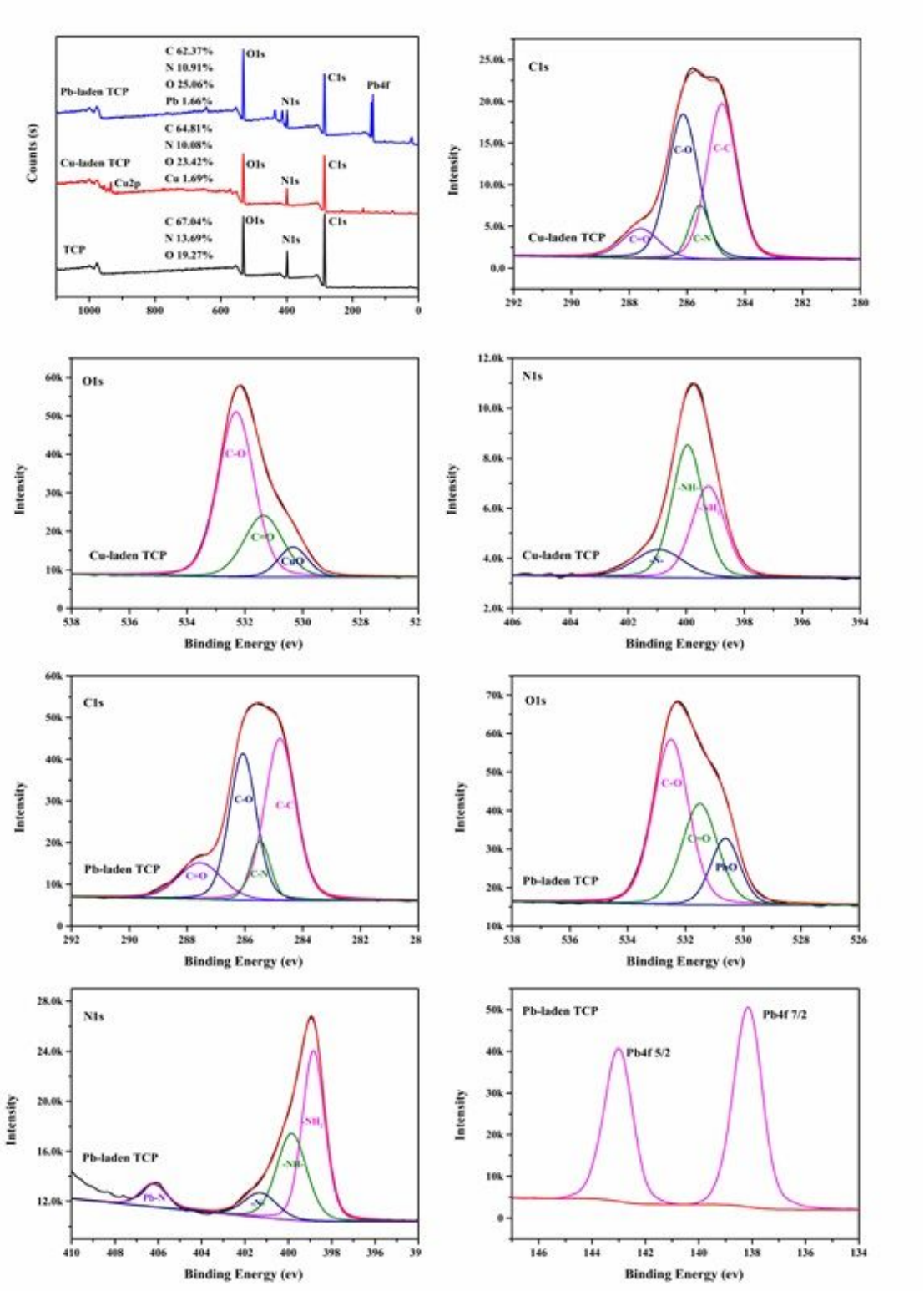

Figure 14

The XPS spectra of TCP before and after adsorption Cu2+ and Pb2+.